

# Low-Power, 8-Channel EEG Recorder and Seizure Detector ASIC for a Subdermal Implantable System

Bruno G. Do Valle, *Member, IEEE*, Sydney S. Cash, and Charles G. Sodini, *Fellow, IEEE*

**Abstract**—EEG remains the mainstay test for the diagnosis and treatment of patients with epilepsy. Unfortunately, ambulatory EEG systems are far from ideal for patients who have infrequent seizures. These systems only last up to 3 days and if a seizure is not captured during the recordings, a definite diagnosis of the patient's condition cannot be given. This work aims to address this need by proposing a subdermal implantable, eight-channel EEG recorder and seizure detector that has two modes of operation: diagnosis and seizure counting. In the diagnosis mode, EEG is continuously recorded until a number of seizures are recorded. In the seizure counting mode, the system uses a low-power algorithm to track the number of seizures a patient has, providing doctors with a reliable count to help determine medication efficacy or other clinical endpoint. An ASIC that implements the EEG recording and seizure detection algorithm was designed and fabricated in a 0.18  $\mu\text{m}$  CMOS process. The ASIC includes eight EEG channels and is designed to minimize the system's power and size. The result is a power-efficient analog front end that requires 2.75  $\mu\text{W}$  per channel in diagnosis mode and 0.84  $\mu\text{W}$  per channel in seizure counting mode. Both modes have an input referred noise of approximately 1.1  $\mu\text{V}_{\text{rms}}$ .

**Index Terms**—Biomedical electronics, biomedical signal processing, electroencephalography, epilepsy, implantable biomedical devices, microelectronic implants.

## I. INTRODUCTION

**E**PILEPSY is a common neurological disorder that affects about 1% of the world population [1]. It is characterized by repeated seizures, which are caused by abnormal neuronal firing in the affected brain area [2]. If the abnormal neural activity is localized in a specific part of the brain, it is called a focal seizure; seizures that involve large portions of the brain at their outset are named generalized. To determine the type of seizure and brain areas involved, an electroencephalogram (EEG) is performed [2]. EEG is the recording of the electrical activity on the scalp. Capturing a seizure with EEG is a necessary prerequisite for making a definitive diagnosis, tailoring therapy, moving

toward certain kinds of solutions such as surgery, or even affixing the true rate of seizures.

Although EEG has been the chief modality in the diagnosis and treatment of epileptic disorders for more than half a century, the vast majority of tests are still performed in hospital or office settings and are of brief duration. Long term recordings (from days to weeks) can be obtained but these must occur in a hospital setting. Many patients have intermittent seizures occurring very infrequently—from once a week to once every few months [3]. These patients cannot come into the hospital for weeks on end in order for an event to be captured on EEG, making an accurate and definitive diagnosis very difficult.

Once the diagnosis is made, neurologists face another major challenge: to obtain the true rate of seizures of the patient to be able to determine if the prescribed medication is working correctly. Currently, doctors rely on patients to track the number of seizures they have, even though it has been shown that patient reports tend to be very inaccurate [4]. However, because neurologists have no other means of getting that information, they have to rely on an inaccurate number when determining whether the dose should be increased/decreased or if the medication should be switched.

## II. BACKGROUND

Currently, EEG systems can record the neuronal activity in the following ways: on the scalp (EEG), using penetrating electrodes (needles that penetrate the skin), or under the skull either on top of the brain (electrocorticography, ECoG) or in the parenchyma itself.

Ambulatory scalp EEG systems, such as the ones presented in [5] and [6], have many drawbacks: they only last up to 3 days, the patient must wear a backpack that contains the recording electronics all the time, the patient cannot shower since water interferes with the electrodes [7], and many avoid daily activities such as work and school while wearing the system given its aesthetics [8].

The invasive solution of placing the electrodes on the brain or implanting them also present challenges. The major one is the requirement of a craniotomy—surgical operation in which a hole is drilled through the skull in order to access the brain. Since this type of surgery is risky and invasive, implantable systems are only used in very specific cases, for example, an attempt to determine the exact focal point of a seizure before surgical procedure to remove that part of the brain.

Invasive systems, such as the ones presented in [9] and [10], typically implant the device package in the skull, place the recording electrodes on top of the brain, and implant a stimulating electrode in the brain. The idea is to detect a seizure as

Manuscript received July 11, 2015; revised November 07, 2015; accepted December 27, 2015. This research was supported by MIT Medical Electronics Device Realization Center and the Center for Integrated Circuits and Systems. This paper was recommended by Associate Editor R. Genov.

B. G. Do Valle and C. G. Sodini are with the Department of Electrical Engineering and Computer Science, Massachusetts Institute of Technology, Cambridge, MA 02139 USA (e-mail: brunogr@mit.edu; sodini@mit.edu).

S. S. Cash is with the Department of Neurology, Massachusetts General Hospital, Boston, MA 02114 USA (e-mail: scash@partners.org).

Color versions of one or more of the figures in this paper are available online at <http://ieeexplore.ieee.org>.

Digital Object Identifier 10.1109/TBCAS.2016.2517039

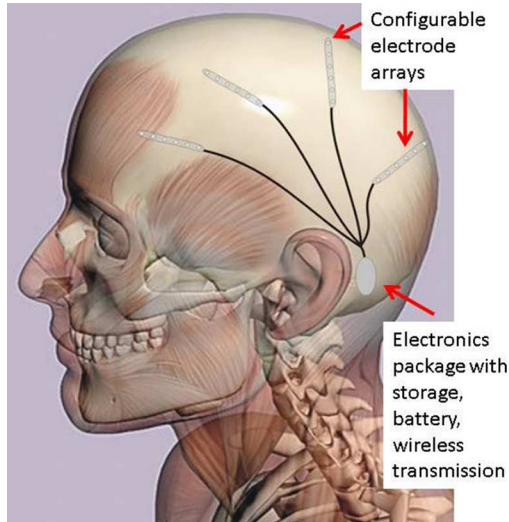


Fig. 1. Subdermal EEG recorder and seizure detector implant [11].

soon as possible from the recorded brain activity and stimulate the brain in order to stop the seizure.

Since ambulatory EEG systems don't last more than a few days and invasive systems require major surgery, we propose a different approach: a minimally invasive system where the device and recording electrodes are implanted subdermally, between the scalp and skull. The system is implanted behind the patient's right or left ear and the electrodes are tunneled underneath the scalp into the desired locations, as shown in Fig. 1. Subdermal recordings have higher signal to noise ratio when compared to surface EEG recordings [12]. As a result, seizure detection algorithms might yield better results [10]. Subdermal EEG recordings is still in its infancy, however, it has great potential to provide better long-term EEG recordings.

The proposed subdermal system has two modes of operation: diagnosis and seizure counting. In diagnosis, the EEG is continuously recorded until at least one seizure is recorded. The recorded seizure(s) is used to train the detection algorithm on the ASIC, so that it can start counting seizures. In seizure counting, the system uses a low-power algorithm to track the number of seizures a patient has. The detection algorithms in the invasive systems presented in [9] and [10] need to detect seizures as fast as possible since they are trying to stop them, thus detection delay is a major concern. On the other hand, our system only counts the number of seizures a patient had during a certain period of time. As a result, detection delay is not a major concern in our case. This fact can be used to significantly reduce the power in our detection algorithm.

In order for a system to be clinically useful in the diagnosis of epilepsy, the channel count must be at least four [13]. A higher channel count provides a greater coverage of the brain, however, it increases the system's power consumption. For this ASIC we decided to use eight channels because it seemed a good compromise between power consumption and brain coverage.

This paper presents the design of a low-power, eight-channel EEG recorder and seizure detector application-specific integrated circuit (ASIC), designed to be used in the minimally invasive implant system. This paper is organized as follows:

Section III describes the system's two modes of operation; Section IV and V present the design of the analog front end and seizure detection algorithm used in the ASIC, respectively; Section VI shows measured results of the ASIC; Section VII concludes the paper.

### III. MODES OF OPERATION

Most EEGs recorded in the hospital are sampled at 256 Hz since the clinical analysis usually focuses on activities below 50 Hz [15]. However, one of the main drawbacks of this sample rate is the lack of high-frequency content (higher than 128 Hz). High-frequency oscillations (HFO), which lie between 100 Hz–500 Hz and typically have amplitudes between  $5 \mu\text{V}$ – $30 \mu\text{V}$ , were shown to be present on some patients at the seizure onset region before the beginning of a seizure [16], [17]. Since a sample rate of 256 Hz is not able to record HFO, it was important that our system sampled the EEG at a frequency higher than 1,000 Hz.

Our system's two modes of operation will be referred to as Mode 1 and Mode 2. Mode 1 is used for diagnosis. In this mode the EEG is sampled at 1,280 Hz, enabling the recording of HFO. The data is continuously transferred to an external device similar to the ones used in cochlear implants. The external device is responsible for receiving the data and transmitting power to the implant through an inductive link. After at least one seizure is recorded, a training set can be created for the detection algorithm and the system can be used in Mode 2: seizure counting mode. The change from Mode 1 to Mode 2 is determined by the physician and is performed by programming the ASIC using the external device. In Mode 2, the system only records ten seconds of EEG after the electrical onset of a seizure is detected by our algorithm. The ten-second segment is recorded so that the physician can confirm whether the algorithm correctly identified a seizure or if it was a false alarm. In Mode 2, the patient only wears the external device for about 15 minutes once a day to recharge the implant's battery and also to receive the seizure data recorded during that day. Since the external device is not continuously worn in Mode 2, the seizure data is stored in a flash memory. To minimize power consumption in Mode 2, the EEG is sampled at a typical clinical setting of 256 Hz and only recorded after our algorithm detects a seizure. The drawback of this approach is that the beginning of a seizure may be missed due to the algorithm's detection delay. However, as mentioned previously, it is not an issue since the use model is to only count the number of seizures. Also, the other approach of buffering the EEG to not miss the beginning of a seizure would consume too much power.

Power is also minimized in the seizure detection algorithm. Instead of having one power-hungry algorithm in the implant that detects all seizures and produces very few false alarms, we have two algorithms: a power-efficient, simple algorithm in the implant, and a complex one in a computer. The power-efficient algorithm in the implant attempts to detect all seizures, but produces a higher number of false alarms than other complex algorithms, such as [10] and [14]. However, all the recorded seizure data is stored and later analyzed in a computer using any complex algorithm, such as the machine learning example presented in [10], to reduce the number of false alarms, making the dataset



TABLE II  
SIMULATED RESULTS OF THE AMPLIFIER

| Parameter                     | Recommended Value                     | Simulated Results Mode 1                | Simulated Results Mode 2                |
|-------------------------------|---------------------------------------|-----------------------------------------|-----------------------------------------|
| Low-Frequency Response        | 0.5 Hz or lower                       | 0.07 Hz                                 | 0.07 Hz                                 |
| High-Frequency Response       | 70 Hz or higher                       | 500 Hz                                  | 100 Hz                                  |
| Noise Level                   | $< 1 \mu\text{Vrms}$<br>(0.5 – 70 Hz) | 0.88 $\mu\text{Vrms}$<br>(0.5 – 500 Hz) | 0.91 $\mu\text{Vrms}$<br>(0.5 – 100 Hz) |
| Input Impedance               | $> 1 \text{ M}\Omega$                 | 1.6 $\text{G}\Omega$                    | 1.6 $\text{G}\Omega$                    |
| Common Mode Rejection (60 Hz) | $> 60 \text{ dB}$                     | 77.8 dB                                 | 77.6 dB                                 |
| Dynamic Range                 | $> 40 \text{ dB}$                     | 60 dB                                   | 60 dB                                   |
| Power Consumption             | N/A                                   | 1.39 $\mu\text{W}$                      | 0.47 $\mu\text{W}$                      |

used large transistors for M1, M2, M7, and M8. The area of M1 and M7 are  $1,400 \mu\text{m}^2$  and  $3,000 \mu\text{m}^2$ , respectively. These values are on the order of 35,000 times higher than the minimum transistor area, which according to (1), reduces the input referred flicker noise power spectral density by a factor of roughly 35,000. The cascode transistors M2, M3, M4, and M5 contribute almost no noise [22]. They were included to increase the gain of the amplifier by increasing the output impedance.

In order to minimize power consumption, the supply voltage was reduced. All transistors in the LNA are in subthreshold, requiring approximately 100 mV between the drain and source to remain in saturation [22]. We have five transistors between VDD and ground, so the minimum supply voltage to have all transistor in saturation is approximately 0.5 V. We also need to take into consideration the voltage swing at the output nodes. The gain of the LNA is set to 120 and the maximum input voltage during a seizure is typically 1 mV [2], thus the output node can swing between +120 mV to -120 mV. In order to keep M3, M4, M5, and M6 always in saturation, regardless of the input voltage, they require at least 220 mV between the drain and source. Therefore, the minimum supply is 740 mV. We decided to set the supply to 0.9 V, so that we are not running the transistors at the edge of saturation.

Table II summarizes the simulated results of the amplifier and compares them to the ACNS's guideline. All of our simulated results exceed the recommended values. In Mode 2 (seizure counting), the bias current and the bandwidth are reduced by a factor of five. This results in total input noise staying practically constant since thermal noise is proportional to bandwidth and inversely proportional to current. The total power consumption is reduced by less than a factor of five because the current used to generate the bias voltages (VBIAS and VBIAS2) was not lowered.

### B. Programmable Gain Amplifier

The second block in the AFE is the programmable gain amplifier (PGA). The top-level schematic is basically the same as the one illustrated in Fig. 2; the only difference is that the input capacitors are variable. Since the LNA's bias current is very small (1.6  $\mu\text{A}$ ) we used capacitors instead of resistors to set the gain in the PGA. If we had used resistors instead, their values would

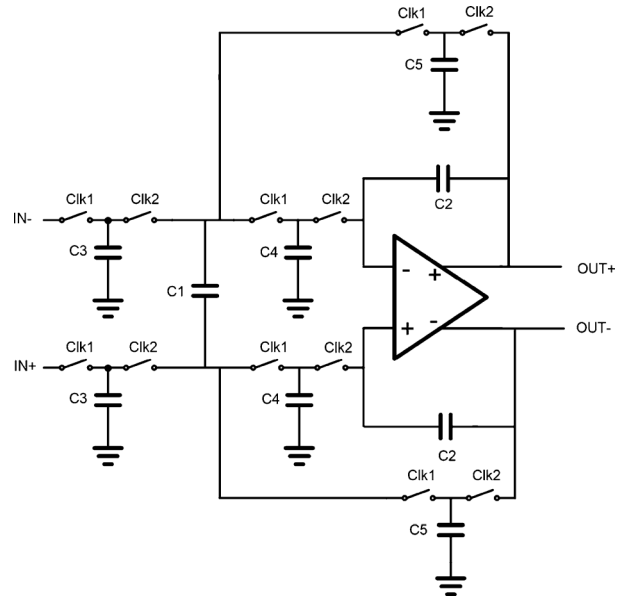


Fig. 4. Rauch filter schematic using switched capacitors to replace resistors.

have to be very large (on the order of tens of  $\text{M}\Omega$ ) in order to not load the output of the LNA, which would have increased noise and also layout area.

The gain of the PGA can be set to four different values: 12 dB, 14 dB, 17.5 dB, and 23.5 dB. With the gain set to 17.5 dB, the PGA will saturate when the LNA input is over 1 mV, which is typically the maximum amplitude during a seizure. The gain setting of 12 dB and 23.5 dB were included so that the input amplitude that causes the PGA to saturate could be changed to 500  $\mu\text{V}$  and 2 mV.

### C. Anti-Alias Filter

The anti-alias filter limits the bandwidth of the signal to avoid aliasing when sampling in the ADC. The ADC sample rate is 5.12 kHz and 1.024 kHz in Modes 1 (diagnosis) and 2 (seizure counting), respectively. Since the resolution of the ADC is nine bits, the required attenuation at half the sampling frequency is 56 dB to ensure that the signal is below the ADC quantization noise. In Mode 1, the bandwidth of interest is 500 Hz, so we need a third-order filter with poles located close to 500 Hz to get the required attenuation. A capacitor was included between the output terminals of the LNA to create a pole located around 650 Hz. As a result, the anti-alias filter only needs to be a second-order low-pass filter (LPF).

A Rauch topology with resistors replaced by switched capacitors was used as the anti-alias filter because it provides a second-order transfer function with reduced sensitivity to component variation [23]. The poles are dependent on the ratio of capacitors, which is not significantly impacted by process variation if common-centroid technique is used in layout. The schematic is illustrated by Fig. 4.

In order to design the Rauch filter to be maximally flat, meaning that the passband will have a flat frequency response like a Butterworth filter, the values of the capacitors need to be

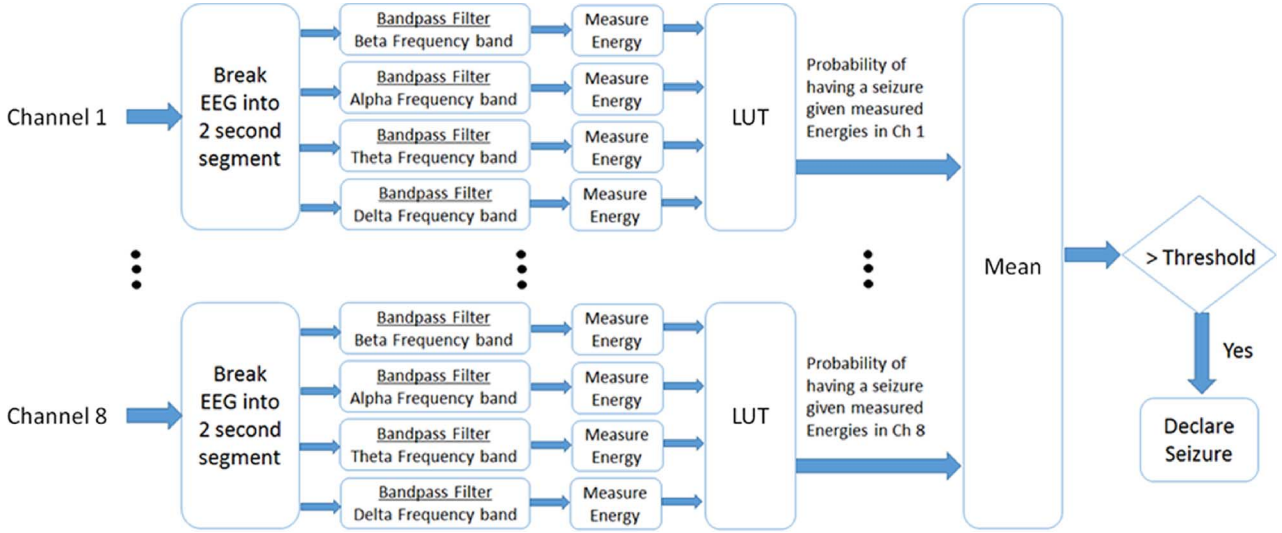


Fig. 5. High level block diagram of proposed seizure detection algorithm.

set according to (2) and (3). The location of the poles are then given by (4) [24].

$$C_1 = 2C_2 = 2C \quad (2)$$

$$C_4 = 2C_3 = 2C_5 = C_{req} \quad (3)$$

$$f_p = \frac{C_{req} f_s}{4\pi C \sqrt{2}} \quad (4)$$

In Mode 1 (diagnosis), the EEG bandwidth of interest is 500 Hz, so the poles were designed to be approximately at 550 Hz to compensate for any clock frequency mismatch or process variation that could push them lower in frequency. In Mode 2 (seizure counting), the bandwidth is reduced by a factor of five, so the poles should be closer to 100 Hz. According to (4), this is easily accomplished by reducing the clock frequency by a factor of five.

The amplifier used in the anti-alias filter was designed as a fully differential two-stage Miller-compensated. The power consumption of the anti-alias filter is  $0.84 \mu\text{W}$  and  $0.20 \mu\text{W}$  in Modes 1 and 2, respectively.

#### D. ADC

The ADC employed in this ASIC was reported in [25]. It is a 9-bit successive approximation register (SAR) ADC with 53.6 dB of SNDR and 8.6 effective number of bits (ENOB). In Modes 1 and 2 the ADC converts 5,120 and 1,024 samples a second, respectively. The ADC oversamples the data by a factor of four in order to increase the resolution from 9 to 10 bits in the digital core. It runs at 0.9 V and consumes 158 nW and 32 nW when in Modes 1 and 2, respectively.

The digital core decimates the EEG data by a factor of four using polyphase filters to reduce computation requirements [26]. The filter was designed using MATLAB's filter design tool, which also generated the FIR Verilog code [27]. The Verilog code was then synthesized into digital logic and included in the ASIC.

TABLE III  
FREQUENCY BANDS USED IN THE ALGORITHM

| Band Name | Frequency Range |
|-----------|-----------------|
| Delta     | 0.5 Hz – 4 Hz   |
| Theta     | 4 Hz – 8 Hz     |
| Alpha     | 8 Hz – 13 Hz    |
| Beta      | 13 Hz – 30 Hz   |

#### V. SEIZURE DETECTION

A power-efficient seizure detection algorithm was also included in the ASIC by synthesizing digital logic. The key feature of the algorithm is that it uses energy in physiological-meaningful frequency bands, shown in Table III, to generate a simple probability value of the patient having a seizure. If the probability is higher than a threshold value determined during training, then a seizure is declared and ten seconds of data are recorded. Fig. 5 shows a top-level block diagram illustration of the proposed four-step algorithm.

The first step in the algorithm is to break down each channel's EEG data into two-second segments since the lowest frequency of interest is 0.5 Hz. Each segment overlaps the next by 50% or one second. Next, the algorithm measures the energy of each two-second segment in the four frequency bands listed in Table III. The energy is calculated by summing the square of the voltage values according to (5), derived from Parseval's theorem. Thirdly, we use the measured energies in a lookup table (generated during patient-specific training) to get a probability value of a seizure taking place. Lastly, we take the mean of the probability output of all channels. The mean value goes through a ten-second moving average filter and is compared with a threshold determined during training. If the moving average output is higher than the threshold, the algorithm flags a seizure and records the data for ten seconds for later analysis.

$$Energy = \sum |x_n|^2 \quad (5)$$

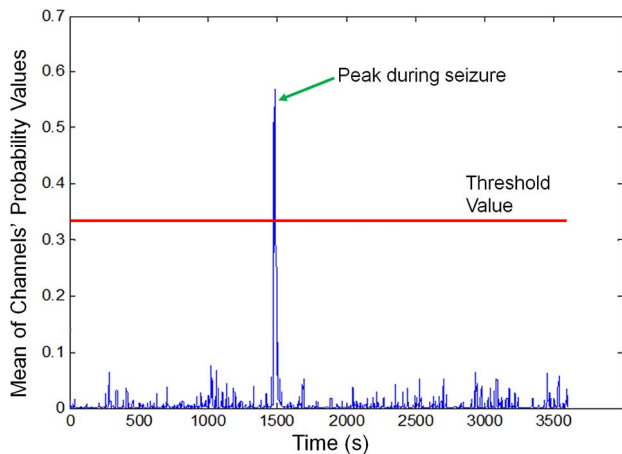


Fig. 6. Probability of having a seizure versus time. Seizure starts at 1467 seconds and ends at 1494 seconds.

### A. Training

During the training phase, we use the data acquired in Mode 1 (diagnosis) to generate a probability lookup table and determine the threshold value. At least one EEG record from the patient, with the seizure's start and end time annotated, is required for this process.

With the training data we follow the four-step procedure described in the previous section. In order to calculate the probability value of having a seizure given a measured energy value 'Energy<sub>n</sub>' we use (6), dividing how often the measured energy value 'Energy<sub>n</sub>' occurs during the seizure by how often it occurs in the entire record.

$$P(\text{Seizure}|\text{Energy}_n) = \frac{P(\text{Seizure and Energy}_n)}{P(\text{Energy}_n)} \quad (6)$$

The threshold value is a percentage of the peak probability value during the seizure in the training record. It is determined by running the training record through our algorithm, which will yield a probability value of having a seizure every second, as shown in Fig. 6. Since we used this record to train, it's no surprise that there is a spike in probability value during the seizure between 1467 and 1494 seconds.

The threshold value can be set at different levels, depending on the accuracy needed. There is an important trade-off when setting it: the higher the value, the lower the number of false alarms and the lower the number of seizures detected.

### B. Bandpass Filters

As mentioned before, the algorithm requires four bandpass filters to measure the energy in the bands listed in Table III. Since we are not concerned with the phase of the signal, we can use IIR instead of FIR filters to significantly save computational requirements. The IIR filters were implemented as Chebyshev Type II in order to minimize the filter order while still keeping the passband maximally flat [26]. After the signal goes through the bandpass filter, the energy during the 2 second segment is calculated using (5).

TABLE IV  
ESTIMATED POWER CONSUMPTION OF THE ALGORITHM'S BLOCKS

| Block        | Estimated Power Consumption (nW) |
|--------------|----------------------------------|
| Delta Filter | 98                               |
| Theta Filter | 89                               |
| Alpha Filter | 77                               |
| Beta Filter  | 107                              |
| LUT          | 108                              |
| Other        | 75                               |
| <b>Total</b> | <b>554</b>                       |

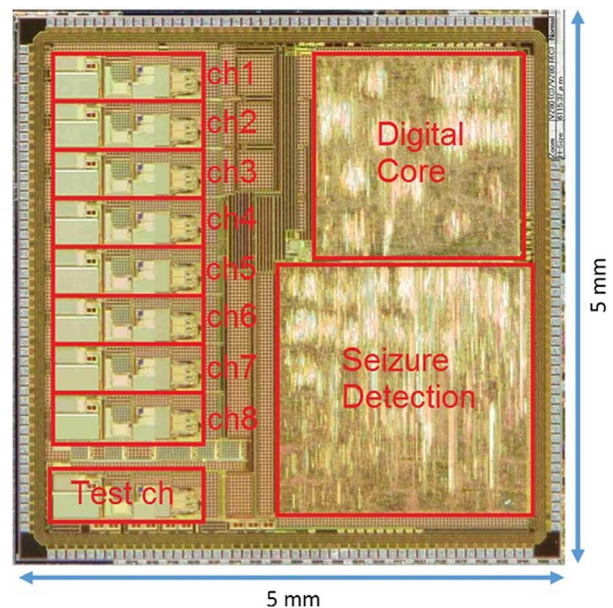


Fig. 7. Die micrograph of the ASIC with circuit blocks labeled.

### C. Probability Lookup Table

The probability lookup table (LUT) contains a probability value of having a seizure for every single possible energy combination ('Energy<sub>n</sub>') from the output of the four bandpass filters. Since this algorithm was implemented in an ASIC, the size of the LUT had to be considered to minimize die area and also power consumption. There are two ways to reduce the size of the LUT: bin the energy value to decrease the number of possible combinations, or only store the probability values of a few combinations. Both methods were used in our algorithm.

To bin the energy, we need to determine the minimum and maximum values and the number of bins to use. Logarithmic binning is used because EEG amplitudes can vary by three orders of magnitude: from 1  $\mu\text{V}$ , typically the noise floor of recording systems, to 1 mV during a seizure [2]. The lowest bin was set to the equivalent energy generated by a 1  $\mu\text{V}$  sine wave during two seconds. Similarly, the highest bin was set to a 1 mV sine wave energy.

The number of bins was set to eight because in preliminary simulations we found that our algorithm had a peak performance at eight bins. Increasing the number of bins increases specificity because it reduces the range of energies that the algorithm will flag as a seizure. At the same time, increasing the number of bins decreases sensitivity because if there is any slight change

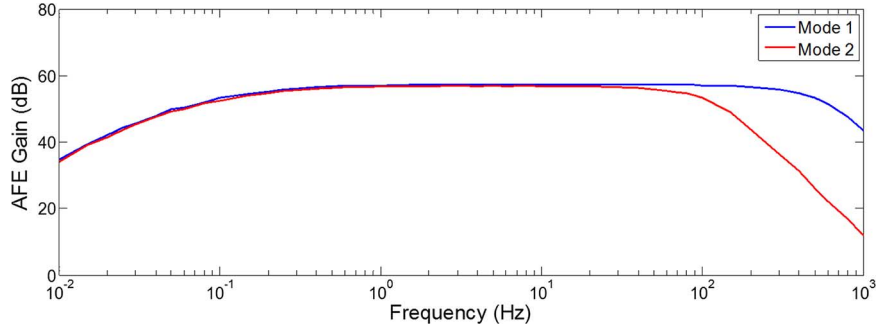


Fig. 8. AFE (from LNA to anti-alias filter) frequency response in Modes 1 (blue) and 2 (red).

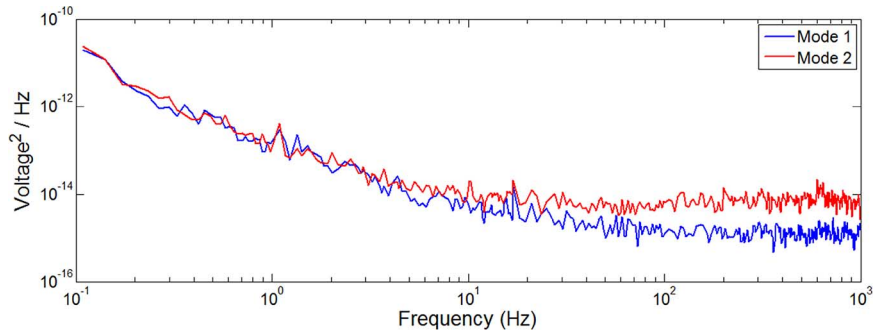


Fig. 9. Input-referred noise power spectral density in Modes 1 (blue) and 2 (red).

in the seizure energy from the training set, the algorithm won't detect it.

Each channel has its own probability LUT. In our case, we have four frequency bands and the energy is discretized into eight bins. As a result, in order to have one entry for every possible combination, we would need 4,096 ( $8^4$ ) rows in the LUT for each channel. Most of the energy combinations are not recorded during a seizure, so there is no need to have one entry for every possible combination. Consequently, we limit the LUT to only fifty rows. After we measure the probability for every possible combination, we only keep the fifty highest probability values, all others are assumed to yield a value of zero. By using a LUT for each channel with only 50 rows instead of 4,096, the area per LUT was reduced from 8.7 mm<sup>2</sup> to only 0.1 mm<sup>2</sup> while the power consumption was reduced from 5.4  $\mu$ W to 108 nW. As for the algorithm's sensitivity, according to simulations, there was no impact reducing the number down to fifty rows. Below fifty rows, sensitivity starts to decrease.

#### D. Estimated Power Consumption

Table IV lists the estimated power consumption of each block according to simulations. The "other" block shown in the table includes the multiplier to measure energy and also some overhead, such as writing and reading from registers, etc. According to Table IV, no block dominates the power consumption—all consume roughly the same percentage.

## VI. MEASUREMENT RESULTS

An ASIC, which measures 5 mm by 5 mm, was fabricated using the TSMC 0.18  $\mu$ m process. A photomicrograph can be seen in Fig. 7.

TABLE V  
MEASURED POWER CONSUMPTION PER CHANNEL IN MODES 1 AND 2

| Block             | Measured Power Mode 1 ( $\mu$ W/ch) | Measured Power Mode 2 ( $\mu$ W/ch) |
|-------------------|-------------------------------------|-------------------------------------|
| AFE               | 2.75                                | 0.84                                |
| Digital Core      | 1.0                                 | 0.44                                |
| Seizure Detection | 0.2                                 | 0.45                                |
| <b>TOTAL</b>      | <b>3.95</b>                         | <b>1.73</b>                         |

#### A. Frequency Response

Fig. 8 plots the frequency response of the LNA, PGA, and anti-alias filter combined. This is the frequency response that the EEG data passes through from the input of the LNA until the input of the ADC. The high-pass response is due to the pseudo-resistors in the LNA. In Mode 2, the poles are shifted from approximately 500 Hz to 100 Hz by changing the clock frequency in the anti-alias filter.

#### B. Noise Measurement

The input-referred noise power spectral density was measured with an Agilent 35670A Dynamic Signal Analyzer in both modes of operation. The result is presented in Fig. 9. In Mode 2, the bias current is reduced by a factor of five, so flicker noise stays constant while thermal noise increases roughly by a factor of five. The total input-referred noise in Modes 1 and 2 are 1.13  $\mu$ V<sub>rms</sub> (0.5–500 Hz) and 1.06  $\mu$ V<sub>rms</sub> (0.5–100 Hz), respectively.

#### C. Power Measurement

Table V compares the measured power consumption per channel in both modes. In Mode 2, the AFE power decreases

TABLE VI  
AFE COMPARED WITH PUBLISHED LITERATURE

| Parameter                                  | [29]                                                 | [14]                                                 | [30]                                                | [31]                                                 | [32]                                                | [33]                                                | [34]                                                | This System                                          |
|--------------------------------------------|------------------------------------------------------|------------------------------------------------------|-----------------------------------------------------|------------------------------------------------------|-----------------------------------------------------|-----------------------------------------------------|-----------------------------------------------------|------------------------------------------------------|
| AFE Power ( $\mu\text{W}/\text{channel}$ ) | 0.69                                                 | 8.25                                                 | 82                                                  | 104                                                  | 1.6                                                 | 1.8                                                 | 6.9                                                 | 2.75                                                 |
| Number of Channels                         | 32                                                   | 8                                                    | 8                                                   | 16                                                   | 16                                                  | 1                                                   | 8                                                   | 8                                                    |
| Supply Voltage                             | 1 V                                                  | 1.8 V                                                | 1.8 V                                               | 1.8 V                                                | 1.8 V                                               | 1.0 V                                               | 3.0 V                                               | 0.9 V                                                |
| CMRR                                       | 83 dB                                                | 90 dB                                                | 84 dB                                               | 102 dB                                               | -                                                   | 134 dB                                              | 120 dB                                              | 78 dB                                                |
| Electrode Offset Rejection                 | Rail to rail                                         | 225 mV                                               | 250 mV                                              | 350 mV                                               | -                                                   | Rail to rail                                        | 45 mV                                               | Rail to rail                                         |
| EEG Bandwidth                              | 150 Hz                                               | 100 Hz                                               | 200 Hz                                              | 100 Hz                                               | 100 Hz                                              | 100 Hz                                              | 315 Hz                                              | 500 Hz                                               |
| Input Referred Noise                       | 1.15 $\mu\text{V}_{\text{rms}}$<br>(0.5 Hz – 150 Hz) | 0.91 $\mu\text{V}_{\text{rms}}$<br>(0.5 Hz – 100 Hz) | 1.8 $\mu\text{V}_{\text{rms}}$<br>(0.5 Hz – 100 Hz) | 0.65 $\mu\text{V}_{\text{rms}}$<br>(0.5 Hz – 100 Hz) | 0.9 $\mu\text{V}_{\text{rms}}$<br>(0.5 Hz – 100 Hz) | 6.7 $\mu\text{V}_{\text{rms}}$<br>(0.5 Hz – 100 Hz) | 0.6 $\mu\text{V}_{\text{rms}}$<br>(0.5 Hz – 100 Hz) | 1.13 $\mu\text{V}_{\text{rms}}$<br>(0.5 Hz – 500 Hz) |
| NEF                                        | 2.2                                                  | 5.1                                                  | -                                                   | -                                                    | 3.3                                                 | 3.3                                                 | 4.3                                                 | 2.2                                                  |
| Technology                                 | 0.35 $\mu\text{m}$                                   | 0.18 $\mu\text{m}$                                   | 0.18 $\mu\text{m}$                                  | 0.18 $\mu\text{m}$                                   | 0.18 $\mu\text{m}$                                  | 65 nm                                               | 0.5 $\mu\text{m}$                                   | 0.18 $\mu\text{m}$                                   |

from 2.75  $\mu\text{W}$  to 0.84  $\mu\text{W}$  because the bias currents in the AFE are reduced. Also, the digital core power goes down from 1  $\mu\text{W}$  to 0.44  $\mu\text{W}$  because the clock frequency running it is reduced. These are the main reasons why Mode 2 consumes less power than Mode 1.

#### D. AFE Comparison

A widely used figure of merit for low-noise amplifiers is the Noise Efficiency Factor (NEF), which was proposed in [28] and described by (7), where  $V_{ni,rms}$  is the input-referred RMS noise voltage,  $I_{total}$  is the total amplifier supply current,  $V_{thermal}$  is the thermal voltage, and BW is the amplifier bandwidth. The measured NEF for our LNA is 2.2.

$$NEF = V_{ni,rms} \sqrt{\frac{2I_{total}}{\pi V_{thermal} 4KT BW}} \quad (7)$$

Table VI compares our AFE with other published results in literature. Our NEF is comparable to state of the art while also operating at a higher bandwidth than the others, enabling the recording of high-frequency oscillation in the EEG.

#### E. Seizure Detection

The EEG database used to measure the performance of the algorithm is the CHB-MIT Scalp EEG Database [35]. It includes 198 seizures and over 800 hours of recorded EEG. The data was collected from 22 patients (5 males, ages 3–22; 17 females, ages 1.5–19) at Children’s Hospital Boston [10].

To estimate the performance of our algorithm on data recorded from a patient, we used the leave-one-record-out validation scheme. In this scheme, we use all seizure records, except for one, to train and test on the record that wasn’t used. The test data was sent to the ASIC through an SPI interface and the ASIC declared every second of data as non-seizure or seizure.

The threshold controls the trade-off between false alarm rate and percentage of seizures detected. Depending on the experi-

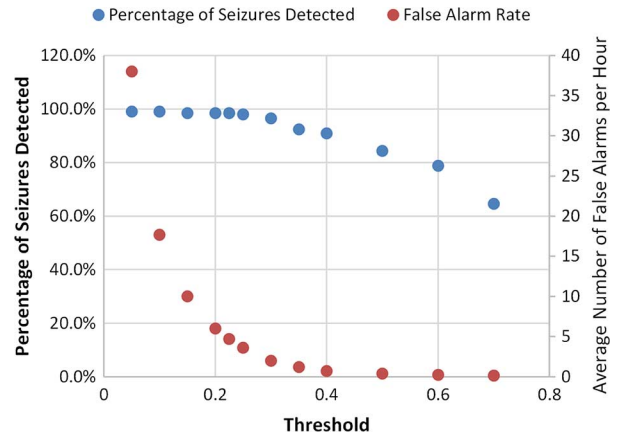


Fig. 10. Percentage of seizure detected and false alarm rate for different threshold values.

ment’s accuracy needs, the threshold value can be changed to satisfy the requirements. Fig. 10 shows how the percentage of seizures detected and false alarm rate vary depending on the chosen threshold. Since the threshold value is stored in a register in the ASIC, it can even be changed during the monitoring if the number of false alarms for a specific patient is deemed too high. The average detection delay, which is the time the algorithm takes to flag a seizure from when it starts, is equal to 9.1 seconds. This latency is not a concern because the algorithm is intended to count the number of seizures—it is not meant to be used as an onset detector. We used a database containing scalp EEG recordings because to the best of our knowledge, there is no subdermal EEG recording database that contains seizures. According to [12], subdermal recordings have a similar power spectral density to scalp recordings, so we expect our algorithm to yield similar results with subdermal recordings.

Table VII compares our seizure detection algorithm results with previous published ones. The threshold was set to 0.25 since according to Fig. 10, this value provides maximal seizure detection without an excessive false alarm rate.

TABLE VII  
COMPARISON OF SEIZURE DETECTION ALGORITHMS

| Parameter                                          | This System | [14]  | [36] | [37] |
|----------------------------------------------------|-------------|-------|------|------|
| Seizure Detection Power ( $\mu\text{W}$ / Channel) | 0.45        | 24.23 | 21.8 | 5.9  |
| % of Seizures Detected                             | 98.5%       | 84.4% | 95%  | 96%  |
| False Alarm per Hour                               | 4.4         | 1.3   | 0.27 | 0.2  |
| # of Channels Used                                 | 8           | 8     | 8    | 18   |

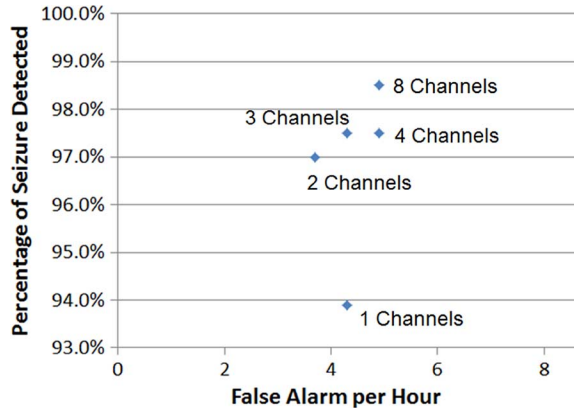


Fig. 11. Algorithm performance for different number of channels used.

Our algorithm consumes over an order of magnitude less power than comparable ones in the literature while still detecting 98.5% of seizures. It does have a higher number of false alarms, which means that we need to store more data to be analyzed than others. In order to estimate the power penalty of having extra data, we used a 128 Mbit flash memory (MX25U12835FZ2I) and measured its power when writing to it at the expected rate. The memory consumes 1.3  $\mu\text{W}$  per channel. Therefore, if we include this power penalty, our algorithm still performs better than the other systems by a factor of three. Even though our algorithm has a higher number of false alarms than other ones, this is not an issue since we can run the stored data through any complex algorithm, such as [10], in a computer to reduce the number of false alarms to a minimal.

#### F. Effect of Number of Channels on Algorithm

Fig. 11 shows the results of the algorithm for using different number of channels: from one to eight. As depicted by the chart, if only one channel is available, the algorithm can still detect approximately 94% of the seizures. This is very encouraging, given the fact that sometimes the electrodes might be placed on areas of the brain barely affected by seizures. Our ASIC can record up to eight channels of EEG, and if the location of the seizure is known and all eight channels are correctly placed, 98.5% of seizures are detected.

## VII. CONCLUSION

This paper presented the design of an ASIC to be used in a minimally invasive subdermal implantable EEG recorder and seizure detector. The ASIC can record up to eight channels of

EEG and uses a power-efficient algorithm to detect seizures. In the diagnosis mode, the ASIC records EEG up to five times the typical bandwidth. The higher bandwidth enables recording of HFO, which can potentially improve diagnosis. The ASIC's low-power consumption enables the design of smaller and better ambulatory EEG systems. It offers patients with epilepsy a more convenient way of monitoring their seizures and gives doctors more accurate information for diagnosis and treatment options.

## ACKNOWLEDGMENT

The authors would like to thank M. Yip for design and layout of the SAR ADC and TSMC for fabricating the ASIC.

## REFERENCES

- [1] W. C. Stacey and B. Litt, "Technology insight: Neuroengineering and epilepsy—Designing devices for seizure control," *Nature Clin. Practice Neurol.*, vol. 4, pp. 190–201, Apr. 2008.
- [2] G. L. Krauss *et al.*, *The John Hopkins Atlas of Digital EEG*. Baltimore, MD, USA: The Johns Hopkins Univ. Press, 2011.
- [3] S. R. Haut *et al.*, "Seizure occurrence: Precipitants and prediction," *Neurology*, pp. 1905–1910, Nov. 2007.
- [4] S. R. Fisher *et al.*, "Seizure diaries for clinical research and practice: Limitations and future prospects," *Epilepsy Behav.*, pp. 304–310, May 2012.
- [5] Lifelines Neurodiagnostic Systems, Ambulatory EEG Systems [Online]. Available: <http://www.lifelinesneuro.com/trackit-aeeeg>, Feb. 1, 2012
- [6] Boston Children's Hospital, Family Education Sheet [Online]. Available: <http://www.childrenshospital.org/~media/Centers%20and%20Services/Departments%20and%20Divisions/Department%20of%20Neurology/AmbulatoryEEG.aspx>, Mar. 22, 2014
- [7] NYU Langone Medical Center, Ambulatory EEG [Online]. Available: <http://epilepsy.med.nyu.edu/diagnosis-treatment/eeeg/ambulatory-eeeg>, Mar. 22, 2014
- [8] Sacred Heart HealthCare System, Ambulatory Electroencephalography (EEG) [Online]. Available: <http://www.shh.org/hospital-services/neurodiagnostic-testing/ambulatory.asp>, Mar. 22, 2014
- [9] B. Lee *et al.*, "A single center experience with the NeuroPace RNS system: A Review of techniques and potential problems," *World Neurosurgery*, Nov. 2014.
- [10] A. Shoeb, "Application of machine learning to epileptic seizure onset detection and treatment," Ph.D. dissertation, Massachusetts Institute of Technology, Cambridge, MA, USA, Sep. 2009.
- [11] Ontario Spinal Institute [Online]. Available: <http://www.ontsi.com/services.htm>, June 2015
- [12] J. Duun-Henriksen *et al.*, "EEG signal quality of a subcutaneous recording system compared to standard surface electrodes," *J. Sensors*, Apr. 2015.
- [13] A. Casson *et al.*, "Wearable electroencephalography," *IEEE Eng. Med. Biol. Mag.*, vol. 29, no. 3, pp. 44–56, Jun. 2010.
- [14] J. Yoo *et al.*, "An 8-channel scalable EEG acquisition SoC with fully integrated patient-specific seizure classification and recording processor," in *Proc. IEEE Int. Solid-State Circuits Conf.*, Feb. 2012, pp. 292–294.
- [15] J. Gotman, "High frequency oscillations: The new EEG frontier?," *Epilepsia*, vol. 51, pp. 63–65, Feb. 2010.
- [16] J. Jirsch *et al.*, "High frequency oscillations during human focal seizures," *Brain*, vol. 129, pp. 1593–1608, Apr. 2006.
- [17] L. P. Andrade-Valencia *et al.*, "Interictal scalp fast oscillations as a marker of the seizure onset zone," *Neurology*, pp. 524–531, Aug. 2011.
- [18] Guidelines for Long-Term Monitoring for Epilepsy, American Clinical Neurophysiology Society, 2008.
- [19] E. Niedermayer and F. L. Silva, *Electroencephalography: Basic Principles, Clinical Applications and Related Fields*. Baltimore, MD, USA: Williams & Wilkins, 2005.
- [20] R. Harrison and C. Charles, "A low-power low-noise CMOS amplifier for neural recording applications," *IEEE J. Solid-State Circuits*, vol. 38, pp. 958–965, Jun. 2003.
- [21] D. Johns and K. Martin, *Analog Integrated Circuit Design*. New York, NY, USA: Wiley, 1996.
- [22] R. Sarpeshkar, *Ultra Low Power Bioelectronics: Fundamentals, Biomedical Applications, Bio-Inspired Systems*. Cambridge, U.K.: Cambridge University Press, 2010.

- [23] B. Ahuja, "Implementation of active distributed RC anti-aliasing/smoothing filters," *IEEE J. Solid-State Circuits*, vol. 17, pp. 1076–1080, Dec. 1982.
- [24] F. Maloberti, *Analog Design for CMOS VLSI Systems*. New York, NY, USA: Springer Science and Business Media, Oct. 2001.
- [25] M. Yip *et al.*, "A 0.6 V 2.9  $\mu$ W mixed-signal front-end for ECG monitoring," in *Proc. Symp. VLSI Circuits*, Jun. 2012, pp. 66–67.
- [26] A. Oppenheim and R. Schaffer, *Discrete-Time Signal Processing*, 3rd ed. Englewood Cliffs, NJ, USA: Prentice Hall, Aug. 2009.
- [27] R. Losada, "Digital filters with MATLAB," *Mathworks*, May 2008.
- [28] M. Steyaert and W. Sansen, "A micropower low-noise monolithic instrumentation amplifier for medical purposes," *IEEE J. Solid-State Circuits*, vol. 22, pp. 1163–1168, Dec. 1987.
- [29] X. Zou *et al.*, "A 1 V 22  $\mu$ W 32-channel implantable EEG recording IC," in *Proc. IEEE Int. Solid-State Circuits Conf.*, Feb. 2010, pp. 126–127.
- [30] J. Xu *et al.*, "A wearable 8-channel active-electrode EEG/ETI acquisition system for body area networks," *IEEE J. Solid-State Circuits*, vol. 49, no. 9, pp. 2005–2016, Sep. 2014.
- [31] J. Xu *et al.*, "A 15-channel digital active electrode system for multi-parameter biopotential measurement," *IEEE J. Solid-State Circuits*, vol. 50, no. 9, pp. 232–247, Sep. 2015.
- [32] M. Altaf *et al.*, "A 16-channel patient-specific seizure onset and termination detection SoC with machine-learning and voltage-mode transcranial stimulation," in *Proc. IEEE Int. Solid-State Circuits Conf., Dig. Tech. Papers*, Feb. 2015, pp. 394–395.
- [33] Q. Fan, F. Sebastiano, J. H. Huijsing, and K. A. A. Makinwa, "A 1.8  $\mu$ W 60 nV/ $\sqrt{\text{Hz}}$  capacitively-coupled chopper instrumentation amplifier in 65 nm cmos for wireless sensor nodes," *IEEE J. Solid-State Circuits*, vol. 46, no. 7, pp. 1534–1543, Jul. 2011.
- [34] R. F. Yazicioglu, P. Merken, R. Puers, and C. V. Hoof, "A 200  $\mu$ W eight-channel EEG acquisition ASIC for ambulatory EEG systems," *IEEE J. Solid-State Circuits*, vol. 43, no. 12, pp. 3025–3038, Dec. 2008.
- [35] A. L. Goldberger *et al.*, "PhysioBank, PhysioToolkit, PhysioNet: Components of a new research resource for complex physiologic signals," *Circulation*, pp. 215–220, 2000.
- [36] M. B. Altaf and J. Yoo, "A 1.83  $\mu$ J/classification, 8-channel, patient-specific epileptic seizure classification SoC using a non-linear support vector machine," *IEEE Trans. Biomed. Circuits Syst.*, pp. 100–101, Feb. 2015.
- [37] M. Shoaib *et al.*, "A compressed-domain processor for seizure detection to simultaneously reduce computation and communication energy," in *Proc. IEEE Custom Integrated Circuits Conf.*, Sep. 2012, vol. 1, pp. 9–12.



**Bruno G. Do Valle** (M'03) received the B.S. (summa cum laude) and M.S degrees in electrical engineering from Boston University, Boston, MA, USA, in 2006 and 2008, respectively.

Currently, he is working toward the Ph.D. degree at the Massachusetts Institute of Technology (MIT), Cambridge, MA, USA. His research interests include low-power analog and mixed-signal VLSI for biomedical applications, seizure detection algorithms, and design of medical ambulatory systems.



**Sydney S. Cash** received the M.D. and Ph.D. degrees from Columbia University, New York, NY, USA.

He gained further clinical training at Massachusetts General Hospital, Boston, MA, USA. Currently, he is an Associate Professor in the Epilepsy Division of the Neurology Department at Massachusetts General Hospital and Harvard University, Cambridge, MA, USA. He is a member of the BrainGate clinical trial team, and codirector of the Department of Neurology NeuroTechnology Trials Unit. The research in his lab is, broadly speaking, dedicated to trying

to understand normal and abnormal brain activity, particularly oscillations, using multi-modal and multi-scalar approaches particular those which allow for recordings to be made at the microscale (e.g., single unit recordings) as well as at the more macro scale. His work includes a focus on the development of novel neurotechnological approaches to help diagnose and treat common and devastating neurological diseases including epilepsy.



**Charles G. Sodini** (M'82–SM'90–F'95) received the B.S.E.E. degree from Purdue University, West Lafayette, IN, USA, in 1974, and the M.S.E.E. and the Ph.D. degrees from the University of California, Berkeley, Berkeley, CA, USA, in 1981 and 1982, respectively.

From 1974–1982, he was a member of the technical staff at Hewlett-Packard Laboratories, where he worked on the design of MOS memory. In 1983, he joined the faculty of the Massachusetts Institute of Technology (MIT), Cambridge, MA, USA, where he

is currently the LeBel Professor of Electrical Engineering. His research interests are focused on medical electronic systems for monitoring and imaging. These systems require state-of-the-art mixed signal integrated circuit and systems with extremely low energy dissipation. He is the cofounder of the Medical Electronic Device Realization Center at MIT. Along with Prof. Roger T. Howe, he is a coauthor of an undergraduate text on integrated circuits and devices entitled *Microelectronics: An Integrated Approach*. He was also a cofounder of SmaL Camera Technologies, a leader in imaging technology for consumer digital still cameras and machine vision cameras for automotive applications. In 1996–1997, he studied the Hong Kong/South China electronics industry and has continued to study the globalization of the electronics industry.

Dr. Sodini has served on a variety of IEEE Conference Committees, including the International Electron Device Meeting, where he was the 1989 General Chairman. He has served on the IEEE Electron Device Society Administrative Committee, was President of the IEEE Solid-State Circuits Society from 2002–2004, and was the Chair of the Executive Committee for the VLSI Symposium from 2006–2014. He also serves on a variety of industry boards.